UNIVERSIDADE DE LISBOA
FACULDADE DE CIÊNCIAS
DEPARTAMENTO DE FÍSICA

Dynamics of Active Polymer Networks

Francisco Cerdeira

Mestrado Integrado em Engenharia Biomédica e Biofísica
Perfil Biofísica Médica e Fisiologia de Sistemas

Dissertação orientada por:
Prof. Doutor Nuno Araújo
Prof. Doutor Pedro Patrício

2019

Acknowledgements

First and foremost, I would like to to express my gratitude to Nuno Araújo for giving me the opportunity to work at CFTC and introducing me to this fascinating topic. It has been a pleasure to work here under his guidance, where his mentoring and hard work have helped me become a better scientist.

I would like to express my deepest gratitude to Pedro Patrício for all he taught me, the advice, and most importantly, the time and patience spent with me on my work. Without him, I feel, this work would be lacking.

I would like to extend my thanks to the people from CFTC that were always reachable and prompt to help, and from whom I learnt a lot. A special thanks to Didier for all the discussions and camaraderie.

Finally, a special thanks to my family and friends for the continuous support throughout the years.

Abstract

The cytoskeleton is an active soft material, comprised and regulated by a vast number of proteins. Conferring structural stability to the cell, it also plays a relevant role in a variety of other cell processes. Its diverse behaviour has made the cytoskeleton an interesting case study in soft matter physics.

In this work, we aim at explaining the distinct rheological properties through the binding and unbinding of cross-linkers. We start with the Gaussian chain model, where we compare results from our numerical simulations with those found in literature. To model the cross-link capable monomers, we first study particle aggregation, implementing a new interaction potential and investigating the role of temperature and cross-linker density in the size of aggregates. By combining the two studies, we start working towards a reticulated polymer network, first studying placement of cross-linkers in the chain and then adding steric repulsion to chain interactions.

This work is a simplified approach to the study of a cross-linked polymer. Despite simple, this model sets the ground for future studies, where more system-specific interactions should be included.

Keywords: cross-linker; cytoskeleton; polymer.

Resumo

O citoesqueleto é um biopolímero, composto e regulado por um vasto número de proteínas. Responsável por uma variedade de processos celulares, entre os quais o movimento, divisão e crescimento celular, é no entanto na estabilidade mecânica que confere à célula que tem a sua principal função.

Avanços em várias técnicas experimentais vieram mostrar um comportamento reológico complexo e diversificado, muitas vezes contrastante com os seus homólogos sintéticos. A procura por um modelo que explique as peculiaridades deste biopolímero tornou-se, nos últimos anos, um dos temas mais ativos na física da matéria condensada mole.

Na base do modelo desenvolvido ao longo deste trabalho está a importância da anexação e separação das diversas cadeias poliméricas na modelação de uma resposta a estímulos externos. Esta dinâmica é promovida por uma variedade de proteínas acessórias as quais designamos de reticulações.

Neste trabalho começámos por introduzir o modelo da cadeia Gaussiana, mostrando a sua equivalência com o modelo mecanicista correspondente ao uso de monómeros pontuais ligados por molas. Provou-se que o modelo computacional implementado reproduzia o comportamento de uma cadeia polimérica que foi previsto, não só neste trabalho, como na literatura.

Em paralelo, estudámos a agregação de partículas, implementando um potencial de interação que visa simular as características de uma reticulação. Após a validação do potencial, investigámos o efeito da temperatura e densidade de reticulações no número de ligações formadas. Mostrámos a existência de intervalos de valores que maximizam esta quantidade para os parâmetros do potencial escolhidos.

Ao combinar os dois estudos feitos foi-nos finalmente possível iniciar a investigação ao modelo reticulado. Após comparar diferentes posicionamentos para a reticulação na cadeia, foram adicionados efeitos estéricos na forma de repulsão entre diferentes cadeias.

Este trabalho corresponde à primeira abordagem de um modelo computacional para um polímero reticulado. Daqui resulta um modelo simples mas fundamentado, o qual deve ser trabalhado no futuro, com a adição de resistência à flexão das cadeias, um estudo mais pormenorizado no uso de repulsão entre cadeias e a adição de uma tensão de cisalhamento.

Palavras-chave: citoesqueleto; polímero; reticulação.

Contents

List of Figures

List of Tables

Nomenclature

Abbreviations

L-J	Lennard-Jones
MD	Molecular Dynamics
MIC	Minimum Image Convention
PBC	Periodic Boundary Conditions

Notation

α	Arbitrary coordinate
Δt	Time step
$\dot{\gamma}$	Shear rate
ε	Depth of the potential well
κ_s	Spring constant
ρ	Density
σ	Stress tensor
τ_B	Inertial relaxation time
Υ	Number of bonds per particle
υ	Distance at which the potential is equal to zero
Ξ	Collective random force ($\Xi_n = \xi_n - \xi_{n-1}$ with $n \in \mathbb{N}$)
ξ	Random force
ζ	Drag coefficient ($\zeta = 1$ throughout this work)
B	End-to-end distance
b	Effective bond length
d_s	Dimension of the embedded space
E_a	Activation energy

$E_{a,b}$	Activation energy (bond breakage)
$E_{a,f}$	Activation energy (bond formation)
f	Force
g	Constant derived from the fluctuation-dissipation theorem ($g = 2\zeta k_B T$)
h	Height of the potential barrier
k	Rate constant
k_B	Boltzmann constant
m	Mass ($m = 1$ throughout this work)
R	Particle position
r	Distance between two particles
r_b	Distance over which we define two particles (monomers) as bonded
r_c	Cut-off distance
r_{min}	Distance at which the potential reaches its minimum
T	Temperature
t	Time
U	Potential
u	Velocity field
w	Width of the potential barrier

Chapter 1

Introduction

To understand the mechanical properties of a cell, and, in turn, of the tissues the cell forms, we look to the cytoskeleton. Spanning the cell body, this active soft material, comprised and regulated by a vast number of proteins, confers structural stability to the cell. The cytoskeleton also plays a relevant role in a variety of cell processes such as motion, growth, division and phagocytosis.

The cytoskeleton is composed of three major structural types of polymers. Each will be formed by the polymerization of a different kind of protein sub-unit and thus have a characteristic size and structure. The actin filaments are flexible helical polymers, made from the protein actin, that organise into a variety of linear bundles, two-dimensional networks, and three-dimensional gels. The microtubules are long, straight, hollow cylinders, much more rigid than the actin filaments. Finally, the intermediate filaments are rope-like fibres, smaller than the microtubules, constituting a very heterogeneous family [1, 2].

Cytoskeleton organisation is also regulated by a myriad of accessory proteins. Among them we have cross-linkable proteins which are responsible for binding different filaments. They do so in different ways, depending on the type of protein. Some are only able to bind tightly apposed filaments, while others work over a wider range of angles [3]. By regulating the density, activity and type of these accessory proteins, cells are able to create different structures without affecting the physical properties of the constituent elements.

Advances in biophysical techniques such as in fluorescence and atomic force microscopy, as well as in optical and magnetic tweezers have led to ever more precise studies on cell rheology [4–6]. Different studies have noted a strong nonlinear increase in the elastic moduli of the network resulting from an increase in strain exerted [7–13]. After this regime of strain stiffening, an increase in compression levels leads to a reversible strain softening behaviour [14, 15]. Although this can be explained by the breaking of individual filaments, it is in the unbinding and, later, the re-binding of the cross-linkers that enable the elasticity of the network to recover so quickly. It has been shown that thermal energy is sufficient to entail cross-linker unbinding events, being responsible for the local rearrangement of the filaments and consequent energy dissipation [9, 11, 16–20]. A nonlinear response in the form of negative normal stress has been also observed. This is quite unusual, with few materials sharing this characteristic, and those who do so, show a very weak response [21–23]. In contrast, in bio-polymer networks, the negative normal stress can be comparable in magnitude to the applied shear [24].

As different experimental approaches are made, several models are devised with its usefulness usually tied to the timescales probed. The diverse behaviour of the bio-polymer network has led to a lack of consensus on a single, general description for the network. Contrasting often with its synthetic counterparts, this has made it an interesting case study in soft condensed matter physics.

We start chapter 2 with a description of the main concepts behind Brownian Dynamics. We introduce

the Langevin equation, used throughout this work to model the motion of the different particles and derive the fluctuation theorem. We make use of an established theory of the Gaussian chain to study the statistical properties of a single polymer chain with a focus on the equilibrium state and under shear. We do this in order to shed light on the intra-particle interactions and use it as a way to validate our code, since analytical solutions can often be found and then compared to our numerical results (fig. 1.1a).

In chapter 3, we develop a suited interaction potential, which is an extension of the Lennard-Jones potential, to study the binding and unbinding of particles in a diluted system. This enables us to model the cross-link proteins and, at the same time, to introduce and test some concepts behind the numerical implementation of such a problem (fig. 1.1b).

Finally, in chapter 4, we tie all this together and study the behaviour of a reticulated network based on the Gaussian chain and interacting through the potential introduced in chapter 3 (fig. 1.1c). By adding steric interactions between different chains, we aim at a more realistic representation of a chain in solution, avoiding unrealistic chain overlapping.

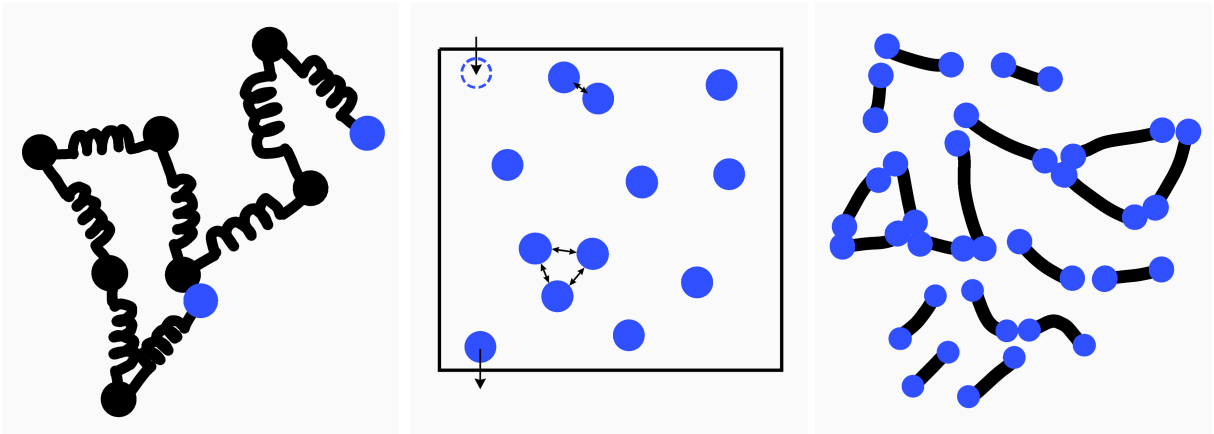

(a) (b) (c)

Figure 1.1: Although slight modifications might be made to suit a specific case study, we present here a simple illustration of the three systems studied in this work. In fig. 1.1a, we have a bead-and-spring system with which we study intra-particle interactions; all particles interact over the same harmonic potential (eq. (2.29)). In fig. 1.1b we show particles enclosed in a box with periodic boundary conditions (section D.3) interacting via a pair potential; this system is used to study inter particle interactions and how they aggregate. Finally on fig. 1.1c, we have a cross-linked network; the blue particles represent cross-linkable proteins of a polymer chain that interact with those of the same kind via the pair potential described earlier (the chain represented in fig. 1.1a corresponds to the two blue “dots” and the black line pair).

Chapter 2

Collective Dynamics of Particles in Solution

Polymers in solution will randomly change their shape and position due to thermal agitation. In this chapter, we study the statistical properties of a single polymer chain in equilibrium; we introduce the Gaussian chain, modelled as a collection of monomers connected by springs, whose motion is taken as a stochastic process, described by a Langevin equation.

The Gaussian chain might not describe correctly the local structure of the polymer but it has the advantage of being much easier to handle from an analytical point of view. Throughout this chapter, we develop an analytical framework, which we use to validate our computational model; from the displacement of a polymer chain, to its viscoelastic properties, we develop the basis of our model.

2.1 Brownian Motion: Langevin Equation

We start by considering the random motion of a large colloidal particle suspended in a fluid. This motion, which results from the collisions with the surrounding molecules of the fluid, can be described as a stochastic process by means of a Langevin equation

$$m\frac{d^2\mathbf{R}}{dt^2} = \mathbf{f}, \tag{2.1}$$

where on the left hand side of the equation we have m as the mass of the particle, R as the position of the particle and t time; on the right hand side we have $\mathbf{f}$, the net force applied on the colloid. It can be split into two contributions: a dissipative one, composed of a deterministic force in the form of a viscous force, $\mathbf{f}_d$, proportional and opposite to the particle velocity

$$\mathbf{f}_d = -\zeta\frac{d\mathbf{R}}{dt}, \tag{2.2}$$

where ζ is the drag coefficient of the particle in the fluid; and a rapidly fluctuating part, that is described as a random force, $\boldsymbol{\xi}$, where for the sake of simplicity and idealisation, we assume a Gaussian process with zero average and its contribution uncorrelated with the particle's motion over long time intervals

$$\langle\boldsymbol{\xi}(t)\rangle = 0; \quad \langle\xi_{\alpha_1}(t_1)\xi_{\alpha_2}(t_2)\rangle = g\delta_{\alpha_1\alpha_2}\delta(t_1 - t_2), \tag{2.3}$$

where α denotes the components of the vector, g is some real constant, $\delta(t_1 - t_2)$ is the Dirac delta function and $\delta_{\alpha_1\alpha_2}$ is the Kronecker delta function. In our work, this stochastic force is the result of the output of a random number generator based on the Mersenne Twister method and defined in the computer program [25]. The reasons for this choice are laid out in appendix B. In order to avoid large numbers that will cause integration problems, a choice is made to truncate the output. The truncation of the Gaussian distribution leads to a shift in the variance that needs to be accounted for. The way this is done is shown in appendix C.

At equilibrium, these two forces relate to each other. In fact, if we multiply both sides of eq. (2.1) by $\mathbf{R}$, and take the average, we will obtain

$$m\frac{d}{dt}\left\langle \mathbf{R}\cdot\frac{d\mathbf{R}}{dt}\right\rangle - m\langle v^2\rangle = -\zeta\left\langle \mathbf{R}\cdot\frac{d\mathbf{R}}{dt}\right\rangle, \tag{2.4}$$

with v being the velocity of the particle. From the equipartition theorem, we know that $\langle v^2\rangle = \frac{d_s k_B T}{m}$, where d_s is the dimension of the embedded space, k_B is the Boltzmann constant and T the temperature. This is a first-order linear non-homogeneous differential equation that can be solved to get

$$\left\langle \mathbf{R}\frac{d\mathbf{R}}{dt}\right\rangle = \frac{1}{2}\frac{d}{dt}\langle R^2\rangle = \frac{d_s k_B T}{\zeta}\left[1-\exp\left(-\frac{t}{\tau_B}\right)\right], \tag{2.5}$$

where $\tau_B = m/\zeta$ is the inertial relaxation time. Integrating a second time yields

$$\langle R^2\rangle = \frac{2d_s k_B T}{\zeta}\left\{t-\tau_B\left[1-\exp\left(-\frac{t}{\tau_B}\right)\right]\right\}, \tag{2.6}$$

and in the limit where the inertial effects can be neglected ($t \gg \tau_B$), we have the motion of the diffusive particle with

$$\langle R^2\rangle = \frac{2d_s k_B T}{\zeta}\,t\,. \tag{2.7}$$

Alternatively, if we neglect the inertial effects, we can write eq. (2.1) as

$$\zeta\,\frac{d\mathbf{R}}{dt} = \boldsymbol{\xi}\,, \tag{2.8}$$

making it much easier to find $\langle R^2\rangle$. Integrating eq. (2.8) yields

$$\mathbf{R}(t) = \frac{1}{\zeta}\int_0^t \boldsymbol{\xi}(t)dt\,, \tag{2.9}$$

meaning that

$$\langle R^2\rangle = \frac{d_s}{\zeta^2}\int_0^t\int_0^t \langle\xi(t_1)\xi(t_2)\rangle\,dt_1 dt_2\,. \tag{2.10}$$

Taking eq. (2.3), we finally get

$$\langle R^2\rangle = \frac{d_s}{\zeta^2}\int_0^t g\,dt_1 = \frac{d_s g}{\zeta^2}t\,. \tag{2.11}$$

Now, we can make use of this result and the one derived through the equipartition theorem, to obtain the fluctuation-dissipation theorem

$$\frac{2d_s k_B T}{\zeta}\,t = \frac{d_s g}{\zeta^2}t \Leftrightarrow g = 2\zeta k_B T\,, \tag{2.12}$$

which relates the variance of the force fluctuations with the temperature of the suspending fluid and the drag coefficient of the particle in it.

2.2 Gaussian Chain

The study of polymers in solution can start with an investigation on the dynamics of a single polymer chain in two dimensions. This simple case corresponds to the limit of diluted solution, where interactions between different polymers chains are negligible.

From a physical standpoint, a polymer can be thought as a set of $N+1$ connected monomers forming a chain. The corresponding bond vectors are defined as

$$\{\mathbf{r}_n\} \equiv (\mathbf{r}_1, \ldots, \mathbf{r}_N)\,, \tag{2.13}$$

with $\mathbf{r}_n = \mathbf{R}_n - \mathbf{R}_{n-1}$, of which $\{\mathbf{R}_n\} \equiv (\mathbf{R}_0, \ldots, \mathbf{R}_N)$ are the position vectors for all monomers.

In our model, the bond vectors are independent of each other, making it possible for a bond to be oriented in every direction, irrespective of the orientation of the others. Accordingly, we allow for the beads, and respective bonds to cross without penalty. The distribution function of the polymer conformation will then be given by

$$\Psi(\{\mathbf{r}_n\}) = \prod_{n=1}^{N} \psi(\mathbf{r}_n)\,, \tag{2.14}$$

where $\psi(\mathbf{r}_n)$ is the normalised distribution of a bond vector

$$\psi(\mathbf{r_n}) = \frac{1}{2\pi b}\delta(|\mathbf{r}_n| - b)\,, \tag{2.15}$$

with b being the effective bond length, that we assume to be the same for all bonds.

Instead of working with all the possible conformations that our polymer chain can have, it becomes more convenient to describe it by its end-to-end vector, $\mathbf{B}$.

$\mathbf{B}$ is a measure of the chain size, that can be easily found experimentally through light scattering techniques. Conversely to the more conventional case, where thermodynamic quantities are expected to show some proportionality to the number of elements, the size of a polymer chain, in thermal equilibrium, yields a different dependence. How the size of a polymer scales as its length is increased, whether it shows a dependence on the temperature or on any other internal or external parameter to the chain, all form interesting questions.

Let the probability distribution function for $\mathbf{B}$ be given by

$$\Phi(\mathbf{B}) = \int \ldots \int_N \delta\left(\mathbf{B} - \sum_{n=1}^{N} \mathbf{r}_n\right) \Psi(\{\mathbf{r}_n\})\, d\mathbf{r}_1 \ldots d\mathbf{r}_n\,. \tag{2.16}$$

Using,

$$\delta(\mathbf{r}) = \frac{1}{(2\pi)^2} \int \exp(i\mathbf{k}\cdot\mathbf{r}) d\mathbf{k}\,, \tag{2.17}$$

and with $\Psi(\{\mathbf{r}_n\})$ given by eq. (2.14), we obtain

$$\begin{aligned}\Phi(\mathbf{B}) &= \frac{1}{(2\pi)^2}\int \exp(i\mathbf{k}\cdot\mathbf{B})\,d\mathbf{k}\int_N \prod_{n=1}^{N}\exp(-i\mathbf{k}\cdot\mathbf{r}_n)\,\psi(\mathbf{r_n})d^n\mathbf{r} = \\ &= \frac{1}{(2\pi)^2}\int \exp(i\mathbf{k}\cdot\mathbf{B})\,d\mathbf{k}\left[\int \exp(-i\mathbf{k}\cdot\mathbf{r})\,\psi(\mathbf{r})d\mathbf{r}\right]^N .\end{aligned} \tag{2.18}$$

The portion of eq. (2.18) that consists of the integral over $\mathbf{r}$ can be evaluated by introducing polar coordinates

$$\frac{1}{2\pi b}\int_0^\infty rdr\int_0^{2\pi}\exp\left[-ikr\cos(\phi)\right]\delta(r-b)\,d\phi = J_0(kb), \tag{2.19}$$

where $k=|\mathbf{k}|$ and $J_0(kb)$ is the Bessel function of the first kind. We consider N to be large, and perform a Taylor expansion of the Bessel function, which leads to

$$\left(1-\frac{(kb)^2}{4}\right)^N \approx \exp\left(-\frac{Nk^2b^2}{4}\right), \tag{2.20}$$

allowing us to write eq. (2.18) as

$$\Phi(\mathbf{B}) = \frac{1}{(2\pi)^2}\int \exp\left(i\mathbf{k}\cdot\mathbf{B}-\frac{N\mathbf{k}^2b^2}{4}\right)d\mathbf{k}. \tag{2.21}$$

This is a Gaussian integral that can be easily solved (section E.2). Taking k_α and B_α, where α denotes the components of the vectors $\mathbf{k}$ and $\mathbf{B}$, we get

$$\begin{aligned}\Phi(\mathbf{B}) &= \frac{1}{(2\pi)^2}\prod_\alpha\left[\int_{-\infty}^{\infty}\exp\left(ik_\alpha\cdot B_\alpha-\frac{Nk_\alpha^2b^2}{4}\right)dk_\alpha\right] = \\ &= \frac{1}{\pi Nb^2}\exp\left(-\frac{\mathbf{B}^2}{Nb^2}\right).\end{aligned} \tag{2.22}$$

The approximation of the distribution function $\Phi(\mathbf{B})$ by eq. (2.22) is what we call the Gaussian Chain. So, we consider a chain whose bond length probability, $\psi(\mathbf{r}_n)$, is a Gaussian distribution given by

$$\psi(\mathbf{r}_n) = \frac{1}{2\pi b^2}\exp\left(-\frac{\mathbf{r}^2}{b^2}\right), \tag{2.23}$$

so that

$$\langle\mathbf{r}^2\rangle = b^2. \tag{2.24}$$

The distribution function of the end-to-end vector is the Gaussian function given in eq. (2.22). This implies that, in the statistics of the Gaussian Chain, the exact bond probability can be replaced by the Gaussian bond probability. As per eq. (2.14), the conformational distribution function of such a chain will be given by

$$\begin{aligned}\Psi(\{\mathbf{r}_n\}) &= \prod_{n=1}^{N}\left[\frac{1}{2\pi b^2}\exp\left(-\frac{\mathbf{r}_n^2}{b^2}\right)\right] = \\ &= \left(\frac{1}{2\pi b^2}\right)^N\exp\left[-\sum_{n=1}^{N}\frac{1}{b^2}\left(\mathbf{R}_n-\mathbf{R}_{n-1}\right)^2\right].\end{aligned} \tag{2.25}$$

An important property of this model will be that the distribution of the vector $\mathbf{R}_n-\mathbf{R}_m$, where n and m

are any two monomers of our chain, is Gaussian and given by

$$\Phi(\mathbf{R}_n - \mathbf{R}_m, n-m) = \frac{|n-m|}{2\pi b^2} \exp\left[-\frac{(\mathbf{R}_n - \mathbf{R}_{n-1})^2}{b^2|n-m|}\right], \tag{2.26}$$

and thus

$$\langle (\mathbf{R}_n - \mathbf{R}_m)^2 \rangle = |n-m| b^2 . \tag{2.27}$$

If we consider the end-to-end vector of a chain with N links to be $\mathbf{B} = \mathbf{R}_N - \mathbf{R}_0$, then eq. (2.27) becomes

$$\langle \mathbf{B}^2 \rangle = N b^2 . \tag{2.28}$$

So far, we considered stiff bonds of fixed length b. We now consider the case where bonds are flexible, with an elastic energy given by

$$U_{\kappa_s}(\{\mathbf{r}_n\}) = \frac{\kappa_s}{2} \sum_{n=1}^{N} \mathbf{r}_n^2, \ \kappa_s = \frac{k_b T}{b^2} . \tag{2.29}$$

Such equivalence can be easily shown. Since we know the distribution function for a single element to be Boltzmann weighted, it follows that

$$\psi(\mathbf{r_n}) \propto \exp\left(-\frac{U_{\kappa_s}}{k_B T}\right) = \exp\left(-\frac{\mathbf{r}_n^2}{2b^2}\right), \tag{2.30}$$

leaving only the normalisation constant, c, to be calculated. Given

$$\int \psi(\mathbf{r}_n) d\mathbf{r}_n = 1 , \tag{2.31}$$

the right-hand side can be simplified as,

$$c \int_0^{2\pi} d\phi \int_0^{\infty} r_n \exp\left(-\frac{r_n^2}{2b^2}\right) = 2\pi c b^2 , \tag{2.32}$$

and so

$$c = \frac{1}{2\pi b^2} , \tag{2.33}$$

meaning that, at equilibrium, we recover the result given by eq. (2.23).

2.2.1 Two-Monomer Chain

Consider a Gaussian chain with two monomers, where the motion for each monomer is determined by the following Langevin equations

$$\zeta \frac{d\mathbf{R}_0}{dt} = -\frac{\partial U_{\kappa_s}(\{\mathbf{r}_1\})}{\partial \mathbf{R}_0} + \boldsymbol{\xi}_0 = \kappa_s (\mathbf{R}_1 - \mathbf{R}_0) + \boldsymbol{\xi}_0 , \tag{2.34}$$

$$\zeta \frac{d\mathbf{R}_1}{dt} = -\frac{\partial U_{\kappa_s}(\{\mathbf{r}_1\})}{\partial \mathbf{R}_1} + \boldsymbol{\xi}_1 = -\kappa_s (\mathbf{R}_1 - \mathbf{R}_0) + \boldsymbol{\xi}_1 . \tag{2.35}$$

Using the bond vector definition, we can rewrite eqs. (2.34) and (2.35) as

$$\zeta \frac{d\mathbf{r}}{dt} = -2\kappa_s \mathbf{r} + \boldsymbol{\Xi} , \tag{2.36}$$

where $\boldsymbol{\Xi} = \boldsymbol{\xi}_1 - \boldsymbol{\xi}_0$, meaning that

$$\langle \boldsymbol{\Xi} \rangle = 0\,, \tag{2.37}$$

$$\langle \Xi_{\alpha_1}(t_1)\Xi_{\alpha_2}(t_2)\rangle = 2g\delta_{\alpha_1\alpha_2}\delta(t_1 - t_2)\,. \tag{2.38}$$

To get the position correlation function, we take eq. (2.36) and express $\mathbf{r}$ in terms of $\boldsymbol{\Xi}$ (see section E.1)

$$\mathbf{r}(t) = \frac{1}{\zeta}\int_0^t \boldsymbol{\Xi}(t_1)\exp\left(-\frac{t-t_1}{\tau}\right)dt_1\,, \tag{2.39}$$

where $\tau = \zeta/2\kappa_s$. Hence

$$\begin{aligned}\langle \mathbf{r}^2(t)\rangle &= \frac{1}{\zeta^2}\int_0^t\int_0^t \langle \boldsymbol{\Xi}(t_1)\cdot\boldsymbol{\Xi}(t_2)\rangle \exp\left(-\frac{t-t_1}{\tau}\right)\exp\left(-\frac{t-t_2}{\tau}\right)dt_1 dt_2 = \\ &= \frac{d_s g}{2\zeta\kappa_s}\left[1-\exp\left(-\frac{4\kappa_s}{\zeta}t\right)\right]\,.\end{aligned} \tag{2.40}$$

The position correlation function can not only offer some insight on the system in question but, with a straightforward implementation, it can also be used as a way to validate our code. By tracking the motion of a large number of particle pairs, we have that their average position, $\langle \mathbf{r}(t)\rangle$, at time t is given by

$$\langle \mathbf{r}(t)\rangle = \frac{1}{N}\sum_{n=0}^{N}\mathbf{r}_n(t)\,, \tag{2.41}$$

where $\mathbf{r}_n(t)$ is the position vector of the n-th particle pair at time t. It follows that the position correlation function is given by

$$\langle \mathbf{r}^2(t)\rangle = \frac{1}{N}\sum_{n=0}^{N}\mathbf{r}_n^2(t)\,. \tag{2.42}$$

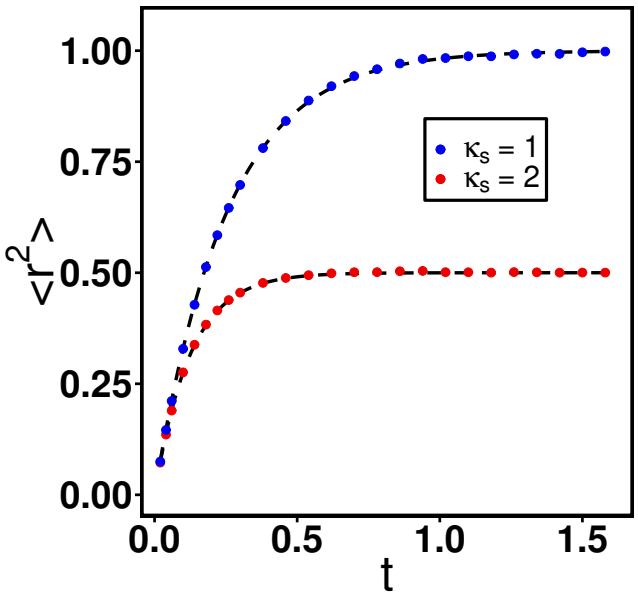

Figure 2.1: With eq. (2.42) we are capable of calculating the position correlation of our two-monomer chain to which we can compare to eq. (2.40), represented by the dashed line. Both methods produce the same result meaning that our code is validated. Parameters used: $g = 1$.

We show in fig. 2.1 that eq. (2.42) is equivalent to eq. (2.40). This is the first step towards validating our computational model, be it the use of the integration method or the truncation of the normal distribution function (see Appendices A and C).

2.3 Viscoelasticity

Polymer solutions have interesting mechanical properties exhibiting both viscous and elastic behaviour and thus being viscoelastic. How those phenomena can be understood from the microscopic characteristic of the materials, their structure and the type of interactions, has been a fundamental question in rheology.

2.3.1 Two-Monomer Chain: Stress Tensor and Viscosity

Suppose that we have a shear flow whose velocity field is given by

$$\mathbf{u}(x,y) = \dot{\gamma} y \hat{\mathbf{i}}, \tag{2.43}$$

where $\dot{\gamma}$ is the shear rate.

The motion of the particle pair will be given by

$$\zeta \frac{d\mathbf{r}}{dt} = \zeta \dot{\gamma} r_y \hat{\mathbf{i}} - 2\kappa_s \mathbf{r} + \boldsymbol{\Xi}, \tag{2.44}$$

where r_y is the y-component of the vector $\mathbf{r}$. Splitting eq. (2.44) into its components we get the following set of equations

$$\begin{aligned} \zeta \frac{dr_x}{dt} &= \zeta \dot{\gamma} r_y - 2\kappa_s r_x + \Xi_x, \\ \zeta \frac{dr_y}{dt} &= -2\kappa_s r_y + \Xi_y, \end{aligned} \tag{2.45}$$

whose solutions, following the steps laid out in section E.1, are

$$\begin{aligned} r_x(t) &= \exp\left(-\frac{t}{\tau}\right) \left[\int_0^t \left(\dot{\gamma} r_y(t_1) + \frac{1}{\zeta} \Xi_x(t_1) \right) \exp\left(\frac{t_1}{\tau}\right) dt_1 \right], \\ r_y(t) &= \exp\left(-\frac{t}{\tau}\right) \left(\frac{1}{\zeta} \int_0^t \Xi_y(t_1) \exp\left(\frac{t_1}{\tau}\right) dt_1 \right). \end{aligned} \tag{2.46}$$

To obtain the effective viscosity of the fluid, we have to determine the stress tensor of the fluid under shear which is obtained through the general expression

$$\sigma_{xy} = \sigma_{xy}^{(s)} + \sigma_{xy}^{(p)}, \tag{2.47}$$

where $\sigma_{xy}^{(s)}$ is the stress tensor due to the solvent and $\sigma_{xy}^{(p)}$ the stress tensor due to the colloidal particles. We focus on the last which is given by

$$\sigma_{xy}^{(p)} = -\frac{c}{N} \sum_{n=0}^{N} \langle f_{n,x} R_{n,y} \rangle, \tag{2.48}$$

where $f_{n,x}$ is the x-component of the force exerted on the n-th particle due to its interactions with all the other colloidal particles [26]. The factor c accounts for the number of segments per volume and, considering we are only working with one chain, $c/N = 1$.

In the case of the simple two monomer chain, the stress tensor is given by

$$\sigma_{xy}^{(p)} = -\langle f_{1,x} R_{1,y} + f_{2,x} R_{2,y} \rangle \,, \tag{2.49}$$

which can be even further simplified by taking into account the bond vector definition and that

$$f_{2,x} = -f_{1,x} = -\kappa_s (R_{2,x} - R_{1,x}) \,. \tag{2.50}$$

Hence, we can have the stress tensor given by

$$\sigma_{xy}^{(p)} = \kappa_s \langle r_x r_y \rangle \,. \tag{2.51}$$

The effective viscosity will be the sum of the fluid viscosity and the viscosity due to the particles,

$$\eta = \eta^{(s)} + \eta^{(p)} \,, \tag{2.52}$$

where the latter is given by:

$$\eta^{(p)} = \lim_{t\to\infty} \frac{\sigma_{xy}^{(p)}}{\dot\gamma} = \frac{\kappa_s}{\dot\gamma} \lim_{t\to\infty} \langle r_x r_y \rangle \,. \tag{2.53}$$

Taking eq. (2.46), we obtain

$$\langle r_x r_y \rangle = \left\langle \left(\exp\left(-\frac{t}{\tau}\right) \int_0^t \dot\gamma r_y(t_1) \exp\left(\frac{t_1}{\tau}\right) dt_1 \right) \left(\frac{\exp\left(-\frac{t}{\tau}\right)}{\zeta} \int_0^t \Xi_y(t_2) \exp\left(\frac{t_2}{\tau}\right) dt_2 \right) \right\rangle \,, \tag{2.54}$$

where the term $\frac{1}{\zeta}\Xi_x(t_1)$ has already been left out since the noise is not only uncorrelated in time but also in space. By taking into consideration eq. (2.3), we also know that its average will be zero and thus, also its contribution. We can further simplify eq. (2.54) by replacing $r_y(t_1)$ once again. We are left with

$$\langle r_x r_y \rangle = \frac{2g\dot\gamma}{\zeta^2} \exp\left(-\frac{2t}{\tau}\right) \int_0^t \int_0^{t_1} \exp\left(\frac{2t_2}{\tau}\right) dt_2 dt_1 \,, \tag{2.55}$$

meaning that the viscosity is given by

$$\eta^{(p)} = \frac{2g\kappa_s}{\zeta^2} \lim_{t\to\infty} \exp\left(-\frac{2t}{\tau}\right) \int_0^t \int_0^{t_1} \exp\left(\frac{2t_2}{\tau}\right) dt_2 dt_1 = \frac{g\zeta}{8\kappa_s} \,. \tag{2.56}$$

We simulated the motion of the particle pair in shear keeping track of its position. After a considerable amount of elapsed time, the x and y components of the bond vector will give the value for $\lim_{t\to\infty}\langle r_x r_y \rangle$. Taking eqs. (2.53) and (2.56), we can express this as

$$\lim_{t\to\infty} \langle r_x r_y \rangle = \frac{g\dot\gamma}{8\kappa_s^2} \,, \tag{2.57}$$

which is very much inline with what one would expect *a priori*.

What we do is nothing more than to measure the x and y components of the pair bond vector, corre-

sponding to the distance between two particles, so it is expected to increase with the temperature, as it was seen in section 2.2.1, and the shear rate, where a larger value means a greater pull, driving the particles apart. On the other hand, the stronger the spring constant, κ_s, the weaker the fluctuations around the equilibrium position.

In fig. 2.2, we vary the spring constant to recover the result in eq. (2.57).

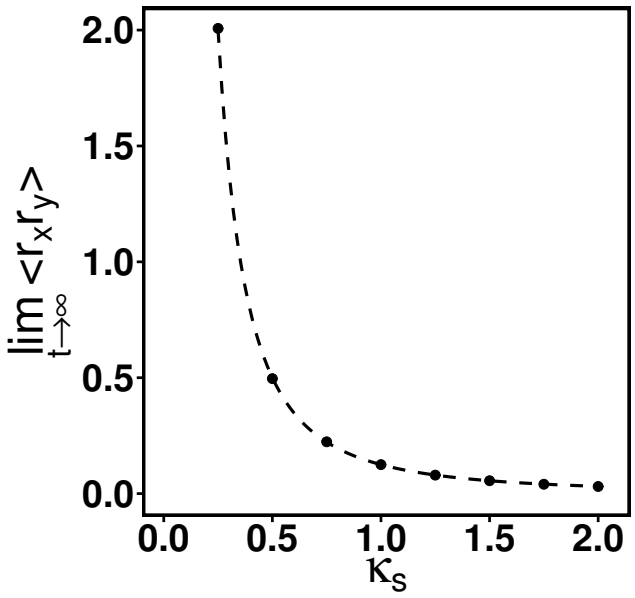

Figure 2.2: From eqs. (2.53) and (2.56) we get eq. (2.57) which we use to check the validity of our code. We place the two monomer chain at the origin and then, under shear, by tracking the position vector of the chain we get the value for $\langle r_x r_y \rangle$ after a considerable amount of time. This can be plotted as a function of the spring constant of the chain, κ_s. We prove that the measurements extracted from our simulated system all fall under the dashed line representing eq. (2.57). Parameters used: $g = 1$, $\dot{\gamma} = 1$.

2.3.2 Effect of Polymer Chain Size

Consider now the role of the size of the polymer chain on the effective viscosity. We know that the motion of the n-th monomer can be determined by the following Langevin equation

$$0 = -\zeta \left(\frac{d\mathbf{R}_n}{dt} - \mathbf{u}(\mathbf{R}_n) \right) - \frac{\partial U_{\kappa_s}}{\partial \mathbf{R}_n} + \boldsymbol{\xi}_n \,, \tag{2.58}$$

meaning that, for a monomer inside the chain, $n \in [2, N-1]$,

$$\zeta \frac{d\mathbf{R}_n}{dt} = \zeta \dot{\gamma} R_{n,y} \hat{\mathbf{i}} + \kappa_s \left(\mathbf{R}_{n+1} - 2\mathbf{R}_n + \mathbf{R}_{n-1} \right) + \boldsymbol{\xi}_n \,, \tag{2.59}$$

whilst, for the extremities,

$$\zeta \frac{d\mathbf{R}_1}{dt} = \zeta \dot{\gamma} R_{1,y} \hat{\mathbf{i}} + \kappa_s \left(\mathbf{R}_2 - \mathbf{R}_1 \right) + \boldsymbol{\xi}_1 \,, \tag{2.60}$$

$$\zeta \frac{d\mathbf{R}_N}{dt} = \zeta \dot{\gamma} R_{N,y} \hat{\mathbf{i}} - \kappa_s \left(\mathbf{R}_N - \mathbf{R}_{N-1} \right) + \boldsymbol{\xi}_N \,. \tag{2.61}$$

Taking $\mathbf{R}_0 = \mathbf{R}_1$ and $\mathbf{R}_{N+1} = \mathbf{R}_N$ allows us to write eqs. (2.60) and (2.61) as eq. (2.59). Making use of the bond vector definition (eq. (2.13)), we can further simplify eq. (2.59) to

$$\zeta \frac{d\mathbf{r}_n}{dt} = \zeta \dot{\gamma} r_{n,y} \hat{\mathbf{i}} + \kappa_s \left(\mathbf{r}_{n+1} - 2\mathbf{r}_n + \mathbf{r}_{n-1}\right) + \boldsymbol{\Xi}_n \,, \tag{2.62}$$

which now holds for $n \in [1, N]$.

From numerical implementation of our Gaussian chain model, we show in fig. 2.3, that $\eta^{(p)}$ scales with N^2, just as predicted in the literature [26]. Since we kept $\dot{\gamma} = 1$, the value for $\eta^{(p)}$ is given by the stress tensor, σ_{xy}, calculated in the final iterations of our simulated system [eq. (2.48)].

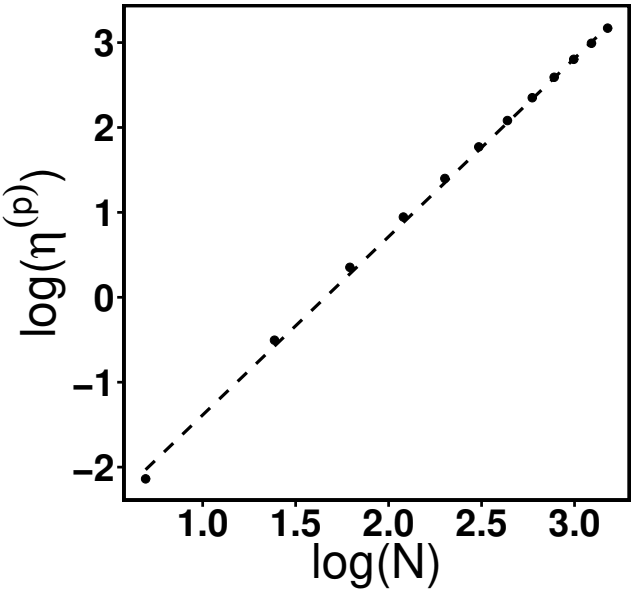

Figure 2.3: By taking a log-log plot of the viscosity due to the particles, $\eta^{(p)}$, in relation to the chain size, N, we show that there is a power law relation. The dashed line, whose slope is ≈ 2, represents the linear regression of the points obtained through numerical simulation. Parameters used: $g = 1$, $\dot{\gamma} = 1$.

Chapter 3

Particle-Particle Aggregation

In this chapter, we study the formation and breakage of bonds. We consider the simplest of models, where N particles placed in a box interact through a pairwise potential.

Potential functions come in many forms but usually provide two important features. First, they account for the resistance to compression, meaning that at a close range, we must have a repulsive force. Secondly, in order to bind particles together, it is necessary to include attraction over a certain range of separation.

3.1 The Lennard-Jones Potential: Initial Look Into Bond Formation

The Lennard–Jones (L-J) potential, originally proposed for liquid argon [27], provides a good starting point for our study. It is given by

$$U_{\text{L-J}} = 4\varepsilon \left[\left(\frac{\upsilon}{r}\right)^{12} - \left(\frac{\upsilon}{r}\right)^{6} \right], \tag{3.1}$$

where r is the distance between particles, ε gives the depth of the well and so it is tied to the strength of the interaction, and υ gives the distance at which the potential is zero [28]. Composed of just two terms, one dominating at short distances, modelling the repulsion between particles, and one attractive one, it became one of the most used potentials in MD for its computational simplicity.

We set a cut-off radius that defines the distance at which the particles can interact (see section D.1). This ensures that the computational effort for one of the more demanding parts of our simulation, the calculation of the force, is reduced. When setting **P**eriodic **B**oundary **C**onditions (PBC) and **M**inimum **I**mage **C**onvention (MIC) we create replicas of our system in all directions and force the particles placed in the main box to interact with the closest particle images available (see section D.3). Failing to set a cut-off radius, or, for that matter, choosing a very small box, leads to numerical errors that arise from particles interacting with themselves since they are able to "reach" their own images.

We follow what is done in the vast majority of MD simulations that consider this potential [28] and set the cut-off radius at

$$r_c = 2.5\, r_{min}\,, \text{ where } r_{min} = 2^{1/6}\upsilon\,. \tag{3.2}$$

The motion of each of these particles will be given by

$$\zeta \frac{d\mathbf{R}_n}{dt} = \boldsymbol{\xi}_n + \sum_{m \neq n} \mathbf{f}_{nm}\,, \tag{3.3}$$

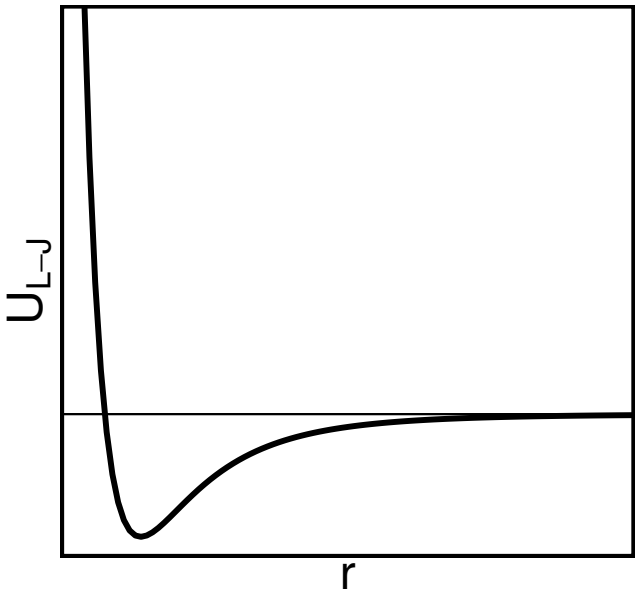

Figure 3.1: Example of a typical Lennard-Jones potential.

where $\mathbf{f}_{nm}$ is the force exerted upon particle n by particle m,

$$\begin{aligned}\mathbf{f}_{nm} &= -\frac{\partial U_{\text{L-J}}}{\partial \mathbf{r}_{nm}} = -\frac{\mathbf{r}_{nm}}{r_{nm}}\frac{\partial U_{\text{L-J}}}{\partial r_{nm}} = \\ &= \left(\frac{\mathbf{r}_{nm}}{r_{nm}^2}\right)\left\{48\varepsilon\left[\left(\frac{\upsilon}{r_{nm}}\right)^{12} - \frac{1}{2}\left(\frac{\upsilon}{r_{nm}}\right)^{6}\right]\right\},\end{aligned} \tag{3.4}$$

with $\mathbf{r}_{nm} = \mathbf{R}_n - \mathbf{R}_m$ as the distance between the two particles.

We first study the effect of temperature on the type of clusters formed, by measuring the number of bonds per particle, Υ, the rate, k, at which those are formed, or broken, and, in a more qualitative manner, the type of structures that are formed.

In order to achieve this, it is imperative that we first define what is a bond. For this simple potential, two particles are bonded if the distance between the two is less than the cut-off radius r_c.

The position of each particle is set at random inside the simulation box, with special care to avoid overlapping. This can be noted in fig. 3.2, where it is shown the initial state as well as the final one, where an equilibrium has been reached. We define this as the time where Υ stays stable.

It was to be expected that an increase in temperature would result in fewer bonds since a decrease in thermal fluctuations will, in theory, trap the particles in the potential well. In fig. 3.3 we show that for a low temperature (fig. 3.3a), a particle will form on average around eleven bonds. Such a high number of bonds was not expected considering that, at short ranges, the particles should repel each other, preventing such highly connected clusters. We notice that by setting the distance as far as r_c led us to count a sort of "next nearest neighbours" as a bond. This is not realistic and is a consequence of a greater problem: the potential chosen.

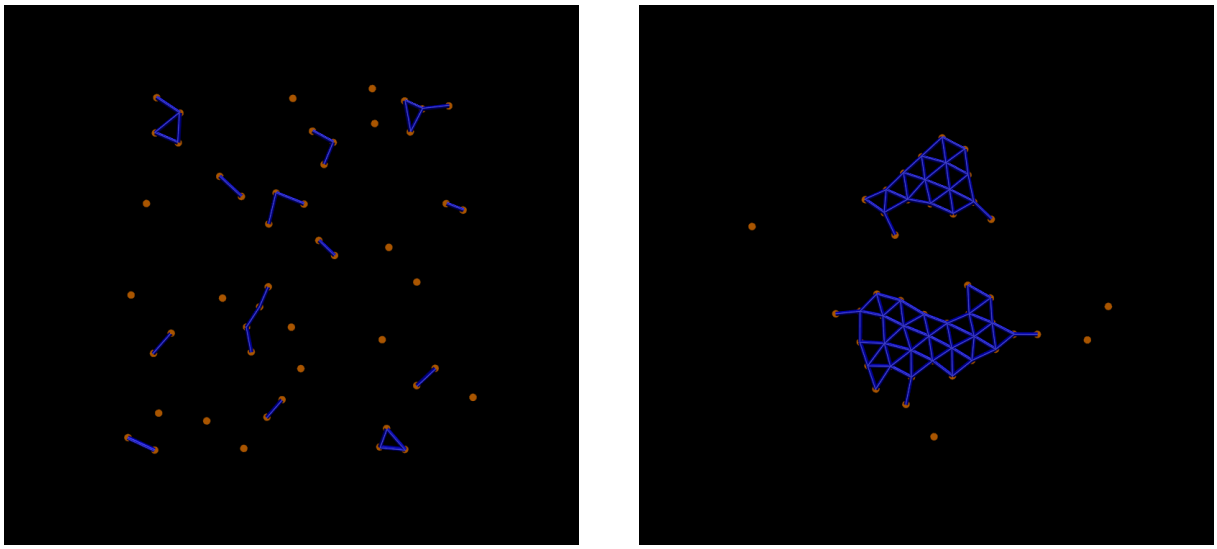

(a) (b)

Figure 3.2: The two images are snapshots of one of the systems studied. The orange "dots" correspond to the particles and the blue "lines" represent the bonds formed by those particles at the time the snapshot was taken. The start of the simulation is shown in fig. 3.2a. The particles are randomly set inside the box, taking measures to avoid overlapping. In fig. 3.2b we show the end of the simulation where an equilibrium in the number of bonds per particle has been reached. Having a visual representation of the system proved to be an invaluable tool in error detection and correction, as well as in the understanding of the system.

3.2 A New Potential: Influence of Temperature and Density on Bond Formation

The L-J potential lacks a activation barrier for the formation of a bond. This is unrealistic and poses a challenge to the definition of a bond.

We address this by adding an exponential to the L-J potential [eq. (3.1)], including a clear cost for the formation of a bond in the form of an energy barrier. We thus define the potential, U_β, as

$$U_\beta = 4\varepsilon\left[\left(\frac{\upsilon}{r}\right)^{12} - \left(\frac{\upsilon}{r}\right)^{6}\right] + h\exp\left[-\frac{(r-r_b)^2}{w^2}\right], \tag{3.5}$$

where h and w are the height and width of the potential wall, respectively, and r_b is the point where we define the formation/breakage of the bond, corresponding to the local maximum of the function (fig. 3.4).

The force will be calculated through the same steps previously described in eq. (3.4) to get

$$\nabla_n U_\beta = \left(\frac{\mathbf{r}_n}{r_n^2}\right)\left\{48\varepsilon\left[\left(\frac{\upsilon}{r_n}\right)^{12} - \frac{1}{2}\left(\frac{\upsilon}{r_n}\right)^{6}\right] + \frac{2h\,(r_n - r_b)}{w^2}\exp\left[-\frac{(r_n-r_b)^2}{w^2}\right]\right\}. \tag{3.6}$$

We start with a simple test on the particle-particle interactions. In one dimension, we fix a particle, allowing another to move, interacting with the previous one through the potential. We can time how long it takes for it to go from the starting distance, which we set as r_{min}, to r_b, meaning, the time it takes for a formed bond to break.

In chemical kinetics, the Arrhenius equation is used to compute the temperature dependence of the reaction rate

$$k = A\exp\left(\frac{E_a}{k_b T}\right), \tag{3.7}$$

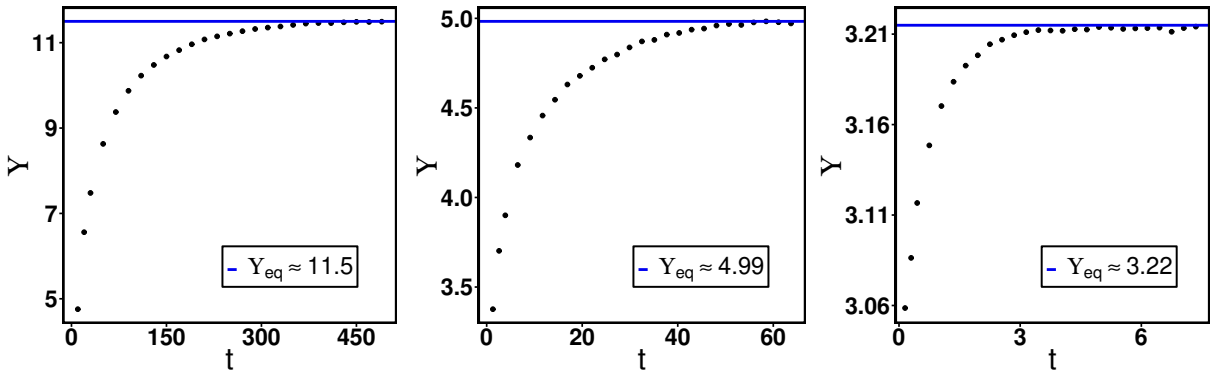

(a) $g = 0.5$ (b) $g = 1$ (c) $g = 2$

Figure 3.3: Comparison between 3 simulations using the L-J potential. We see that as the temperature increases, the number of bonds each particle makes and the time the system takes to reach an equilibrium position, *i.e.* the relaxation time, decrease. We can also observe a very high Υ_{eq} for the case of fig. 3.3a. Parameters used: $\upsilon = 1$, $\varepsilon = 1$, $\rho = 2/15$ [eq. (3.11)].

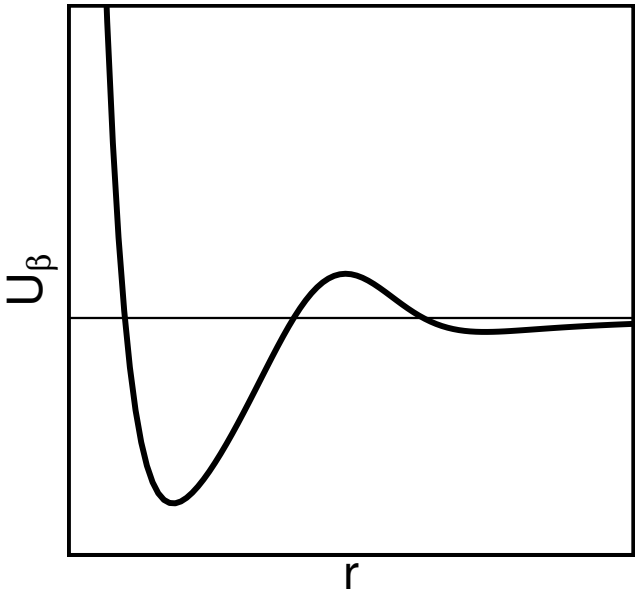

Figure 3.4: Example of the new potential based on the L-J with an additional Gaussian curve

where k is the rate constant, A is some pre-exponential factor and E_a is the activation energy, which is the minimum energy necessary in order to form a bond.

For a single rated-limited activated process, the plot of the logarithm of a reaction rate against the inverse of the temperature will give a straight line whose slope can be used to find E_a.

$$\log(k) = \log(A) + \frac{E_a}{k_B}\frac{1}{T}. \tag{3.8}$$

If we define our rate constant k as the average time needed for our particle to escape the potential well, by varying g, the activation energy for a bond to break, $E_{a,b}$, should correspond to the difference in energy between our starting point, r_{min}, and the point where the particle breaks its bond, r_b. Substituting g into eq. (3.8) we obtain

$$\log(k) = \log(A) + 2\zeta E_{a,b}\frac{1}{g}. \tag{3.9}$$

The value of the potential will depend on the parameters used and on where we define the distance at which we set the barrier. In order to facilitate a comparison to fig. 3.5, the same parameters are used.

The expected activation energy, $E^t_{a,b}$, will be

$$E^t_{a,b} = U_\beta(r_b) - U_\beta(r_{min}) = 1.445\,, \tag{3.10}$$

in units of ε.

From fig. 3.5, we know that the value of the slope is close to $E^t_{a,b}$. The small deviation from the expected value is due to the fact that, for some samples, the simulation time was not long enough for the bond to break

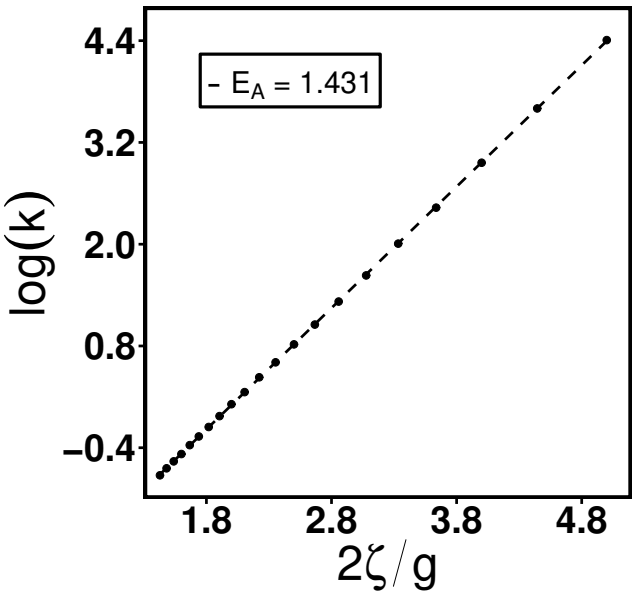

Figure 3.5: In 1D, we time how long a particle takes to reach r_b after it was initially set at r_{min}. After this has been sampled numerous times and the results averaged out, the temperature is increased and the process repeated. By plotting the logarithm of the rate at which the bonds are broken against the temperature change, the resulting slope should give the potential difference between the two points (eqs. (3.9) and (3.10)). Parameters used: $\upsilon = 1$, $\varepsilon = 1$, $h = 0.8$, $w = 0.15$, $r_b = 1.52$.

By shortening the distance at which we define the particles as bonded, we can immediately expect that the number of bonds formed will fall when compared to the previous case shown in fig. 3.3. It is however interesting to note that it appears to exist a sort of optimal g for which Υ_{eq} is maximum and that, past a certain point, the increase in g does not seem to lead to a significant change in Υ_{eq}. As a result of the small number of cases studied, the exploratory study made with the L-J potential [eq. (3.1)] failed to show this behaviour.

We explain this phenomenon by a simple rule: the increase/decrease in the magnitude of thermal fluctuations results in an increase/decrease in the probability of a particle crossing the potential barrier laid out before it. There are two different limiting behaviours: for a low g, thermal fluctuations are small enough to trap the system in its initial configuration, meaning that the rate at which bonds are formed/destroyed is much smaller; for a high g, thermal fluctuations become large enough to make the potential well/barrier negligible, so particles will form and break bonds without a clear cost for it, since the random thermal forces will dominate over their interactions with the other particles in the medium. The fact that we observe a maximum at $g \approx 0.5$ is due to the difference in cost between forming a bond (low cost) and breaking it (high cost) [eq. (3.5)].

In fig. 3.7, we compare the rate, k, at which bonds are formed and broken for different g. We observe that the rates k_{formed} and k_{broken} are indeed much smaller for a low g in an equilibrium regime, solidifying our previous conclusion. Another thing to note is the time scale in which this process occurs, showing

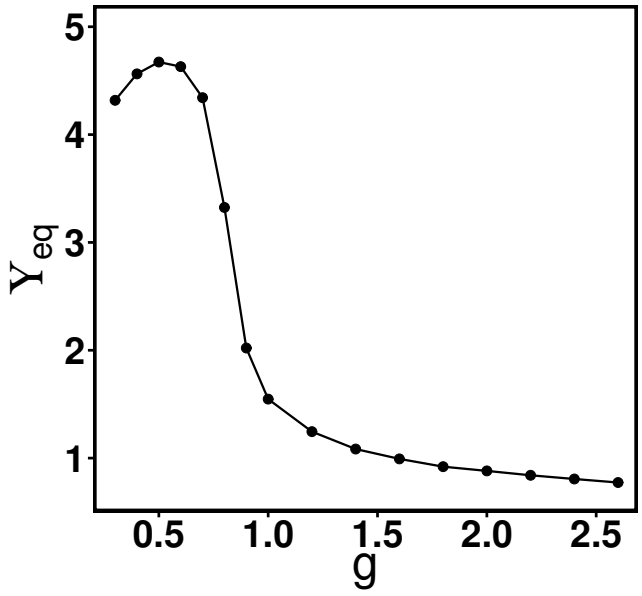

Figure 3.6: We show here the effect temperature has on the number of bonds formed. In its initial state, all particles are placed at random with the only condition being no overlapping. We then let the system relax until a state where the number of bonds formed is kept more or less the same, Υ_{eq}. We show that, for the parameters used, there is a optimal g at which Υ_{eq} is maximum. This is most likely explained by the rate for the formation and breakage of bonds, which is in turn a result of the type of potential used. Parameters used: $\upsilon = 1$, $\varepsilon = 1$, $h = 0.8$, $w = 0.15$, $r_b = 1.52$, $\rho = 2/15$.

that for low g, the system takes much longer to reach an equilibrium state between the two rates (k_{formed} and k_{broken}), leading to a greater number of bonds formed (fig. 3.6).

Let us now focus on the effect of the density, defined as

$$\rho = \frac{N}{A}, \tag{3.11}$$

where A is the area of our enclosing box and N is the number of particles. Driving the choice of density used were the rules we set for the initial state of the system and the amount of events that were observed. Regarding the first case, we set a maximum to how closely we could pack the particles since otherwise, the time to generate the initial configuration would diverge when approaching the jammed state. The second case refers to the fact that at low ρ the number of bonds formed is very low, with the particles wandering in the free space available meaning the system will take much longer to form bonds and converge to a stationary state.

In fig. 3.8 we show the relation between Υ_{eq} and ρ. Two distinct regimes are observed with a soft transition between the two. We note that, for small ρ, Υ_{eq} increases linearly. As the space where particles can diffuse freely gets tighter, they are "forced" to come together and form bonds. For $\rho \gtrsim 0.35$, the decay in Υ_{eq} may be explained by a diminishing kinetic energy caused by a balancing act between the thermal motion and the energy cost of closing in on multiple particles. In other words, their motion is set to a minimum due to interactions with neighbouring particles.

We have discussed the necessity of adding a cost to the formation of a bond. We now observe that it has led to a smaller Υ_{eq}, as predicted; that, in spite of an initial assumption on the role played by temperature and density, there is not a direct relation to the size of aggregates formed and that this behaviour is in part explained by the potential barrier added. It is important to note that by keeping a low density of particles, the computational time can be reduced considerably.

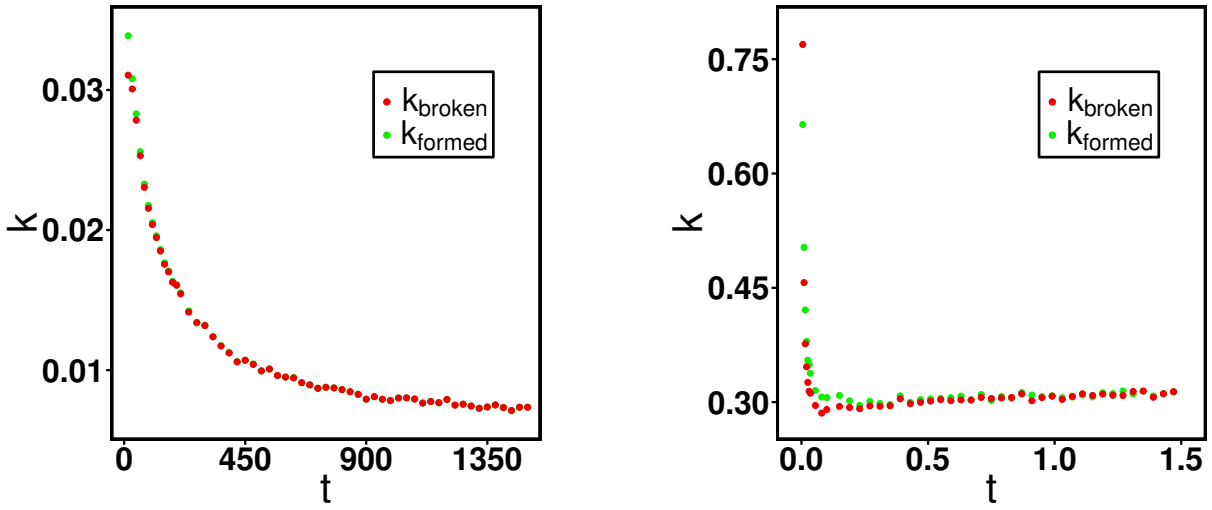

(a) $g = 0.60$ (b) $g = 1.50$

Figure 3.7: The effect of temperature on the rates for bond formation and breakage. We show that for $g = 0.60$ it takes much longer to reach the equilibrium state where k_{formed} and k_{broken} are equal. We observe that, before this occurs, $k_{formed} > k_{broken}$, showing that from our initial state, we would see a rise in Υ . We also note that the rate of either events is lower in the case of $g = 0.6$, by a factor of 10. This was to be expected since the energy cost for both events is kept the same for both cases ($E_{a,b} = 1.445$ and $E_{a,f} = 0.502$). What is shown can serve as an addendum to fig. 3.6, giving valuable insight to better understand the results there shown. Parameters used: $\upsilon = 1$, $\varepsilon = 1$, $h = 0.8$, $w = 0.15$, $r_b = 1.52$, $\rho = 2/15$.

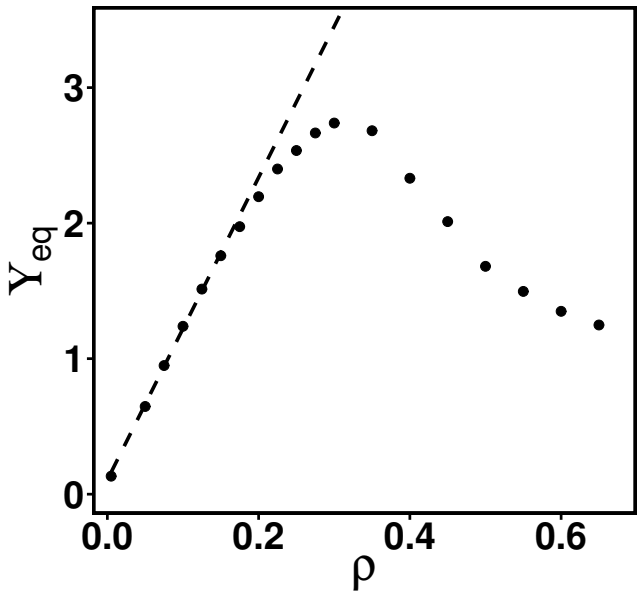

Figure 3.8: The effect of particle density, ρ, on the number of bonds formed. We use a high density of particles throughout this work in order to reduce the amount of computational time it takes for a system to reach its relaxed state. Note the linear relation between the two quantities for low ρ used in the rest of this work. Parameters used: $g = 1$, $\upsilon = 1$, $\varepsilon = 1$, $h = 0.8$, $w = 0.15$, $r_b = 1.52$.

Chapter 4

Crosslinked Polymer Networks

In this chapter we aim at combining what has been learnt throughout the previous chapters, namely, to go from two distinct models to one that is capable of representing the cross-linked nature of these bio-polymers. We will focus on two distinct setups, resulting from the different placement of cross-linkers across the polymer chain.

Consider a five-monomer chain where, as in section 2.2, the monomers interact via an harmonic potential (eq. (2.29)). The different chains will only interact through their cross-linkers, allowing for the overlap of all other monomers. The potential, U_β, introduced in chapter 3 (see eq. (3.5)) will be used to model such cross-link interactions.

We first look at the addition of a cross-linker monomer in the middle of the chain. Note that, by using eq. (2.29), we have that all the particles of a chain will experience a pull towards the centre, and the chain will act as one big colloidal particle, in a system which will, undoubtedly, resemble the one presented in chapter 3.

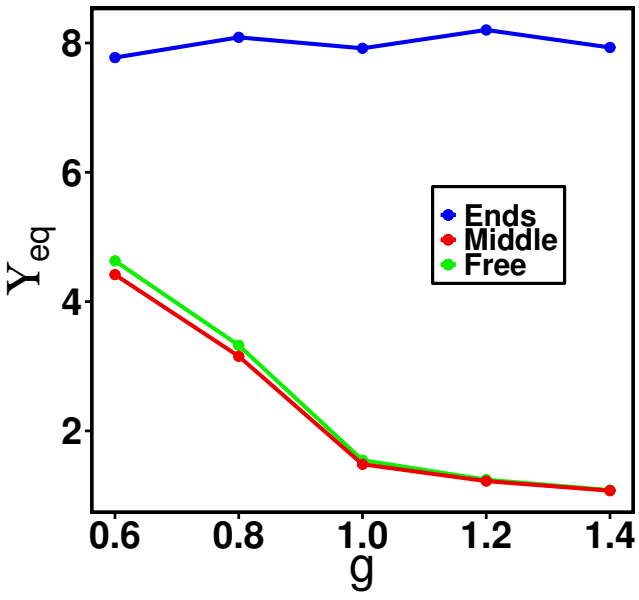

Figure 4.1: Comparison between three models: free particle, five monomer chain with one cross-linker placed at the centre and five monomer chain with two cross-linker placed at ends. The first two cases experience roughly the same behaviour since, in the limit where $\kappa \to \infty$, they should be equal. By placing the cross-linkers at the extremities of the chain, we appear to have created a more stable network, where Υ_{eq} remains the same independently of g. Parameters used: $\kappa_s = 5$, $\upsilon = 1$, $\varepsilon = 1$, $h = 0.8$, $w = 0.15$, $r_b = 1.52$, $\rho = 2/15$.

Placing the cross-linkers at the ends of the chain might make us expect that the different chains

would pull one another, which in turn would lead to their extension. What actually happens is that the different chains get pulled together to form larger clusters. More often then not, when two cross-linkable monomers form a bond, their chain counterparts rapidly comply to completely connect the two chains. Setting the density of cross-linkers constant between the two models, we now expect that the number of bonds per cross-link to be greater in the second since it is easier to "pull" chains together. This is indeed what happens. In fig. 4.1, we see that the system with the cross-linker monomer in the middle of the chain behaves very similarly to the free colloidal particle model. When comparing the two, Υ_{eq} is lower when $g < 1$ for the case of the polymer chain. Moreover, the time it takes for the system to reach a stationary state (not shown here) is longer. The results might be explained by the higher drag which is produced by the rest of the chain, hindering the movement of the cross-linker and consequently its ability to form bonds. What is surprising is the stability of Υ_{eq} to the change of g in the case where the cross-linkers are place at the ends of the chain. The behaviour can be explained if we consider the structures formed that were previously discussed. By having a second cross-linker connecting the two different chains, it becomes harder for them to detach once the bonds are formed, for even if one breaks, the chain will still be in the surrounding perimeter and it can reattach itself. What will happen is that the time for the system to relax from a disordered state might be different but, at least for the systems tested, they will reach a similar relaxed state.

By choosing to ignore interactions between monomers of different chains, we have constructed a rather unrealistic representation of polymer chains in solution. These steric effects are very common and so, to complement the previous model, a repulsive force arising from all interactions between monomers of different chains is added. We chose the L-J potential (eq. (3.1)) for this effect, since, by truncating it at r_{min}, we are able to consider only its repulsive part. Adding to this fact, the L-J potential had already been used throughout this work making its implementation in the model straightforward.

From here, we focus on two different cases: with the cross-linker placed in the middle, it would make sense that, as two chains approach, their ends would bend backwards, allowing for the two cross-link capable monomers to form a bond, connecting their respective chains; in the case of the two cross-linker monomers placed at the ends of the chain, we would expect that, either the two chains in question would extend, allowing for the connection of all cross-linkers or, it would foster connections between more than two chains, since one end of each chain would be able to connect and then, the repulsion between non cross-link capable monomers from both chains, would drive the other end away, making it free to form other connections.

This does not appear to happen. In fig. 4.2 we have the final state of simulations for both cases under the same conditions of fig. 4.1. Even without a plot quantifying Υ_{eq}, a qualitatively analysis of fig. 4.2a shows very few bonds formed. This result is explained by the gathering of monomers around the centre of the chain, promoted by the spring potential introduced in section 2.2, whose equilibrium position is zero. Repulsion will now dominate, making the cross-link attractive potential negligible and keeping the two monomers from establishing a bond. We still notice the expected behaviour but at a much smaller scale. In fig. 4.2b, we notice a strange behaviour. The two cross-linkers from each polymer chain overlap each other. What appears a similar structure to that formed in fig. 4.2a, is in fact a chain connected by its two end points, with its core extended outwards. This doubles the attractive potential while at the same time keeps the repelling monomers at bay, allowing for more bonds to be formed.

In fig. 4.3, we draw a comparison between the two models with cross-linkers placed at the ends of the chain. The addition of repulsion between chains seems to have brought back a transition between a regime that favours bond formation and another that does not. As the temperature increases, so do random motions, making it harder for the chains to arrange, and maintain, the repelling core away from

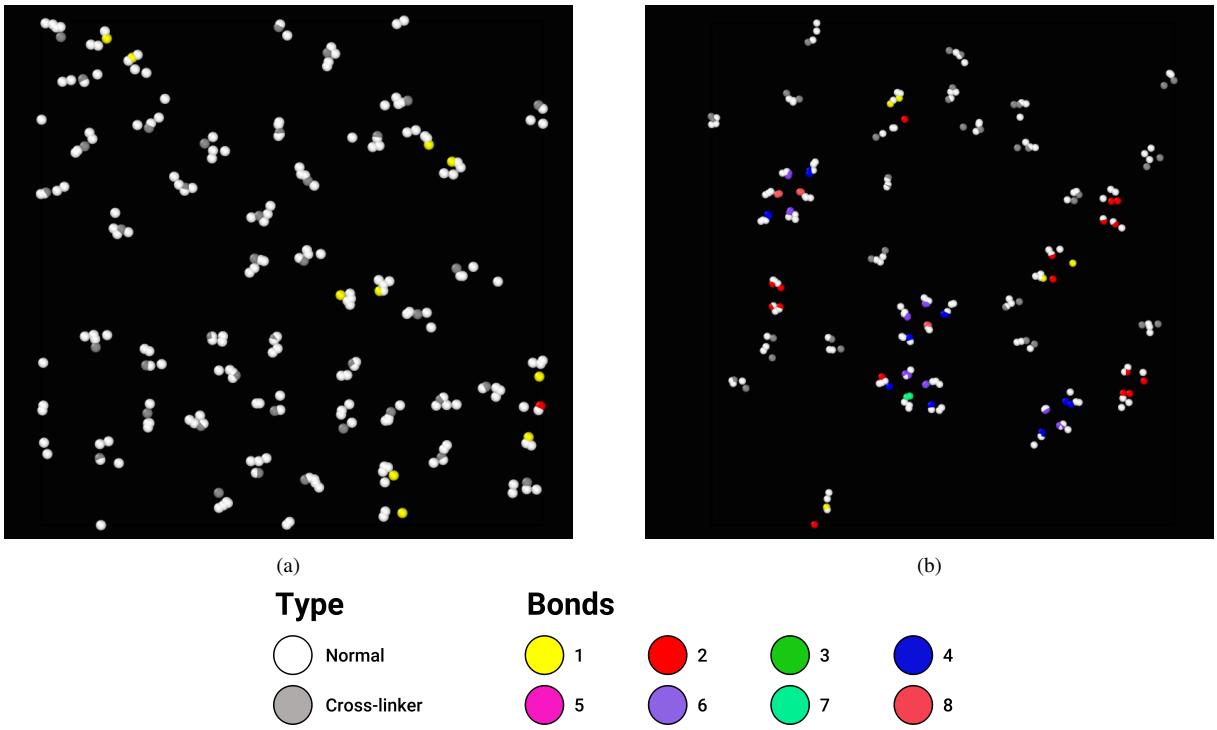

Figure 4.2: Final iteration of the numerical simulation based on the model that considers repulsion between monomers of different chains. In fig. 4.2a, cross-linkers are placed in the middle of the chain. We note that only a small portion of chains are able to form a link. This becomes all the more evident when we look at fig. 4.2b, where the cross-linkers were placed at the ends of the chain. In addition to the higher number of chains interacting and bonds being formed, we observe a new behaviour, with the overlapping of cross-linkers and the chain repelling core pointing outwards. Parameters used: $\kappa_s = 5$, $\upsilon = 1$, $\varepsilon = 1$, $h = 0.8$, $w = 0.15$, $r_b = 1.52$, $\rho = 2/15$.

the cross-linkers attractive potential.

We showed that the placement of the cross-linker in the chain has a direct influence on the size and stability of the network formed. With the addition of repulsion between different chains, we can still recover a regime with a high number of bonds formed, however, under those conditions, instead of the overarching network first envisioned, we observe multiple isolated clusters.

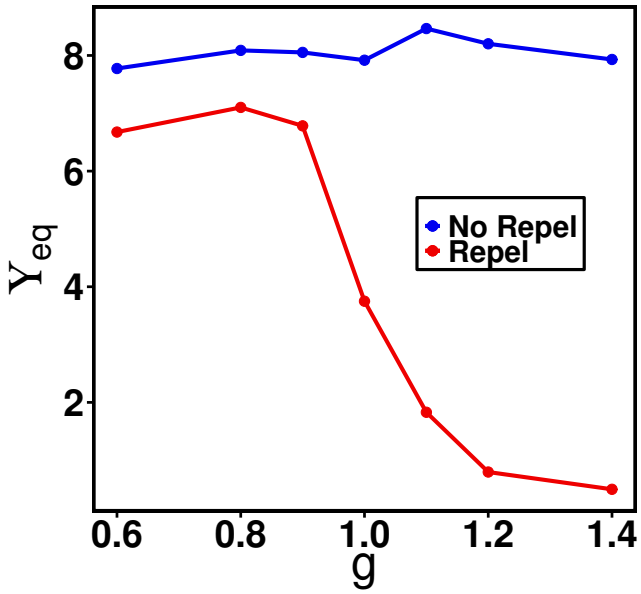

Figure 4.3: Comparison between two different models: with repulsive interactions between monomers of different chains and without; cross-linkers are placed at the ends of the chains in both cases. We note again a transition between two regimes, occurring faster and at a higher g than the one presented in fig. 4.1 for the free particle/middle placement of the cross-linker. Parameters used: $\kappa_s = 5$, $\upsilon = 1$, $\varepsilon = 1$, $h = 0.8$, $w = 0.15$, $r_b = 1.52$, $\rho = 2/15$.

Chapter 5

Conclusions

With this work, we started a study on the dynamics of cross-linked polymer networks. In spite of the complexity of polymer molecules, some general properties can be described by simple models.

We begin by introducing the concepts behind the Gaussian chain, showing its equivalence to a mechanical representation of monomers connected by springs. We verify that for a two monomer chain, the numerical results for the mean square displacement, $\langle r^2 \rangle$, and the intrinsic viscosity due to the placement of the polymer chain in the medium, $\eta^{(p)}$, are in agreement with the theoretical predictions. It was also shown that the relation between $\eta^{(p)}$ and chain size N obtained from our numerical model is inline with what is reported in the literature. These were crucial steps that needed to be taken in order to validate our approach.

The cross-linker properties were then studied as pair interactions between particles confined to a box. From the initial L-J potential used, another one was devised that could more closely match the desired features. After its validation, we studied bond formation under different conditions, showing how it can be influenced by temperature, T and density, ρ, and noting optimum values for which we get a maximum in number of bonds formed.

From here, we begun the construction of our polymer network model, first studying cross-linker placement, from where we noted stark differences between the two versions tested. A middle placement of the cross-linker was used as a bridge to the free particle model, validating the initial assumption of their equivalence. After, we tested placing two cross-linker monomers at the extremities of the chain, where preliminary results show the creation of a much more stable polymer network.

The addition of steric repulsion between different chains was then implemented as we aimed for a more real representation of a polymer in solution. With it, we noted an anomalous behaviour of the different polymer chains, in which they would overlap the cross-link capable monomers, driving the repelling core away. This pushes us away from a reticulated polymer network spanning all space, into small clusters of chains, disconnected from each other.

Future work should then focus on tackling this problem. We first note the repulsion potential used. It served as an initial approach to the problem whose main advantage was its simple and fast numerical implementation. It is then entirely possible that most suitable ways to model these interactions exist.

Steric interactions are not limited to repulsion between different chains but arise from the overlapping of same chain monomers. It is then imperative to add a resistance to bending, making the overlapping of the end monomers more costly. In order to avoid numerical errors, there might also be a need to change the equilibrium position of the spring. By having the monomers very closely packed, a small change in position might lead to a large change in angle and resulting restoring force.

A study of the polymer network under shear conditions is also lacking. From the difficulty to imple-

ment Lees-Edwards boundary conditions, and the refinement of the model, not enough time was left to tackle this case.

If, in the future, this is implemented, we have made it easy to actively change the potential parameters to fit the new conditions. It is possible to change the activation energy for bond formation in respect to the external forces applied. A final thought can be spared to the possibility of a three dimensional model. If this ought to be implemented, it would make sense to add torsional resistance to the chain.

This work was an initial, and therefore, a rather simplistic approach to the system under study. Nevertheless, it gives a good insight on the fundamentals of a cross-linked polymer network, providing a solid base from which we can build upon.

Bibliography

1. Alberts, B. *Molecular Biology of the Cell* Sixth. 889-962 (Garland Science, Taylor and Francis Group, New York, NY, 2015).
2. Hardin, J. & Bertoni, G. *Becker's World of the Cell* Nineth. 375-427 (Pearson, Boston, 2016).
3. Courson, D. S. & Rock, R. S. Actin Cross-Link Assembly and Disassembly Mechanics for Alpha-Actinin and Fascin. *Journal of Biological Chemistry* **285,** 26350–26357 (2010).
4. Mohammed, D. *et al.* Innovative Tools for Mechanobiology: Unraveling Outside-In and Inside-Out Mechanotransduction. *Frontiers in Bioengineering and Biotechnology* **7,** 162 (2019).
5. Kollmannsberger, P. & Fabry, B. High-Force Magnetic Tweezers with Force Feedback for Biological Applications. *Review of Scientific Instruments* **78,** 114301 (2007).
6. Mas, J., Richardson, A. C., Reihani, S. N. S., Oddershede, L. B. & Berg-Sørensen, K. Quantitative Determination of Optical Trapping Strength and Viscoelastic Moduli inside Living Cells. *Physical Biology* **10,** 046006 (2013).
7. Lin, Y.-C. *et al.* Origins of Elasticity in Intermediate Filament Networks. *Physical Review Letters* **104,** 058101 (2010).
8. Schopferer, M. *et al.* Desmin and Vimentin Intermediate Filament Networks: Their Viscoelastic Properties Investigated by Mechanical Rheometry. *Journal of Molecular Biology* **388,** 133–143 (2009).
9. Gardel, M. L. Elastic Behavior of Cross-Linked and Bundled Actin Networks. *Science* **304,** 1301–1305 (2004).
10. Piechocka, I. K. *et al.* Multi-Scale Strain-Stiffening of Semiflexible Bundle Networks. *Soft Matter* **12,** 2145–2156 (2016).
11. Gardel, M. L. *et al.* Stress-Dependent Elasticity of Composite Actin Networks as a Model for Cell Behavior. *Physical Review Letters* **96,** 088102 (2006).
12. Kang, H. *et al.* Nonlinear Elasticity of Stiff Filament Networks: Strain Stiffening, Negative Normal Stress, and Filament Alignment in Fibrin Gels. *The Journal of Physical Chemistry B* **113,** 3799–3805 (2009).
13. Koenderink, G. H. *et al.* An Active Biopolymer Network Controlled by Molecular Motors. *Proceedings of the National Academy of Sciences* **106,** 15192–15197 (2009).
14. Lee, H., Ferrer, J. M., Lang, M. J. & Kamm, R. D. Molecular Origin of Strain Softening in Cross-Linked F-Actin Networks. *Physical Review E* **82,** 011919–011919 (2010).
15. Chaudhuri, O., Parekh, S. H. & Fletcher, D. A. Reversible Stress Softening of Actin Networks. *Nature* **445,** 295–298 (2007).

16. Lieleg, O., Schmoller, K., Claessens, M. & Bausch, A. Cytoskeletal Polymer Networks: Viscoelastic Properties Are Determined by the Microscopic Interaction Potential of Cross-Links. *Biophysical Journal* **96,** 4725–4732 (2009).

17. Tharmann, R., Claessens, M. M. A. E. & Bausch, A. R. Viscoelasticity of Isotropically Cross-Linked Actin Networks. *Physical Review Letters* **98,** 088103 (2007).

18. Semmrich, C., Larsen, R. J. & Bausch, A. R. Nonlinear Mechanics of Entangled F-Actin Solutions. *Soft Matter* **4,** 1675 (2008).

19. Lieleg, O., Claessens, M. M. A. E., Luan, Y. & Bausch, A. R. Transient Binding and Dissipation in Cross-Linked Actin Networks. *Physical Review Letters* **101,** 108101 (2008).

20. Xu, D. & Craig, S. L. Strain Hardening and Strain Softening of Reversibly Cross-Linked Supramolecular Polymer Networks. *Macromolecules* **44,** 7478–7488 (2011).

21. Lin-Gibson, S., Pathak, J. A., Grulke, E. A., Wang, H. & Hobbie, E. K. Elastic Flow Instability in Nanotube Suspensions. *Physical Review Letters* **92,** 048302 (2004).

22. Montesi, A., Peña, A. A. & Pasquali, M. Vorticity Alignment and Negative Normal Stresses in Sheared Attractive Emulsions. *Physical Review Letters* **92,** 058303 (2004).

23. Ciferri, A. *Liquid Crystallinity in Polymers: Principles and Fundamental Properties* (Wiley, 1991).

24. Conti, E. & MacKintosh, F. C. Cross-Linked Networks of Stiff Filaments Exhibit Negative Normal Stress. *Physical Review Letters* **102,** 088102 (2009).

25. Matsumoto, M. & Nishimura, T. Mersenne Twister: A 623-Dimensionally Equidistributed Uniform Pseudo-Random Number Generator. *ACM Transactions on Modeling and Computer Simulation* **8,** 3–30 (1998).

26. Doi, M. & Edwards, S. *The Theory of Polymer Dynamics* (Clarendon Press, 1988).

27. Jones, J. E. On the Determination of Molecular Fields. II. From the Equation of State of a Gas. *Proceedings of the Royal Society A: Mathematical, Physical and Engineering Sciences* **106,** 463–477 (1924).

28. Allen, M. P. & Tildesley, D. J. *Computer Simulation of Liquids* Second. 626 pp. (Oxford University Press, Oxford, United Kingdom, 2017).

29. Ermak, D. L. A Computer Simulation of Charged Particles in Solution. II. Polyion Diffusion Coefficient. *The Journal of Chemical Physics* **62,** 4197–4203 (1975).

30. Ermak, D. L. & McCammon, J. A. Brownian Dynamics with Hydrodynamic Interactions. *The Journal of Chemical Physics* **69,** 1352–1360 (1978).

Appendices

Appendix A

Integration Method

Compared to established techniques for solving deterministic equations of motion, the methods for solving stochastic equations are a great deal less developed.

The most straightforward algorithm is based on the first-order Euler method for ordinary differential equations. Unfortunately, it requires a very small time step to produce sufficiently accurate results, making it highly inefficient [29, 30]. We opt for a Runge-Kutta based algorithm with added stochastic terms. Despite the greater complexity, by requiring more than one evaluation of the force acting upon each particle at a given moment, we can achieve comparable results with a significant larger time step, thus reducing significantly the computing time required.

Consider eq. (A.1), a form of the Langevin equation used throughout this work.

$$\zeta \frac{d\mathbf{r}}{dt} = \mathbf{f} + \boldsymbol{\xi} \,, \tag{A.1}$$

where $\zeta \frac{d\mathbf{r}}{dt}$ is the viscous force, $\mathbf{f}$ is some external force and $\boldsymbol{\xi}$ gives the thermal noise. We discretize eq. (A.1) as follows

$$\begin{aligned} \mathbf{r}(t+\Delta t) &= \mathbf{r}(t) + \frac{\Delta t}{\zeta}\left\{\frac{1}{2}\left[\mathbf{f}(\mathbf{r}(t)) + \mathbf{f}(\mathbf{r}^*(t+\Delta t))\right] + \boldsymbol{\xi}\right\}, \\ \mathbf{r}^*(t+\Delta t) &= \mathbf{r}(t) + \frac{\Delta t}{\zeta}\left[\mathbf{f}(\mathbf{r}(t)) + \boldsymbol{\xi}\right]. \end{aligned} \tag{A.2}$$

where $\boldsymbol{\xi}$ is one random number set by the computer with known mean and variance.

Appendix B

Pseudo-Random Number Generator

The force resulting from the collision of the fluid molecules with the Brownian particle, $\boldsymbol{\xi}$, is regarded as a stochastic variable with a Gaussian distribution.

This creates a need to introduce randomness to our computer program. However, there is no trivial way to make a computer do something by chance, since, by definition, a computer is made to follow instructions and is, therefore, completely predictable. Instead, we make use of pseudo-random numbers.

If we consider a function $f : S \to S$, where S is a finite set of states, and an output function $g : S \to T$, where T is the output space. We define

$$\begin{aligned} S_n &= f(S_{n-1}), \quad n \in \mathbb{N}, \\ T_n &= g(S_n), \end{aligned} \tag{B.1}$$

and, by providing an initial value S_0 for the state, the seed, we can generate a sequence of numbers whose properties approximate, but are not equal to, the properties of sequences of truly random numbers.

Pseudo-random number generators (PRNGs) are an efficient way of producing a large quantity of numbers in a short time, and even its deterministic nature can be useful for it allows to reproduce a certain sequence of numbers, and by implication, a certain experiment, if the seed is known. Unfortunately, PRNGs are also periodic. By using a finite state space, at some point a previous state will be reached and the sequence will repeat itself. This is far from a desirable characteristic but the majority of modern PRNGs have a period long enough that it can be ignored for most practical purposes.

Despite this, the output from many commonly used PRNGs exhibit artefacts that cause them to fail many statistical pattern-detection tests, with shorter periods for some seed states, non uniform distributions and correlation of consecutive values, among others.

In this work, the Mersenne Twister method is used [25]. Although not without some flaws, as it is neither particularly fast nor space efficient, it passes most statistical tests, with a large period which, combined with its straightforward implementation in C++, makes it a good choice for the application in question.

Appendix C

Truncated Normal Distribution

Consider the standard normal distribution, where the probability distribution function of a random variable X is given by

$$\phi_X(x) = a_X \exp\left(-\frac{x^2}{2}\right), \tag{C.1}$$

with $a_X = 1/\sqrt{2\pi}$ and $x \in \,]-\infty, +\infty[$.

We introduce a new random variable Y, based on the previous distribution but truncated at $|Y| < t$, This will have the following distribution

$$f_Y(y) = \begin{cases} a_Y \exp\left(-\frac{y^2}{2}\right) & \text{if } |y| < t \\ 0 & \text{if } |y| > t \end{cases}, \tag{C.2}$$

where normalisation requires that

$$a_Y = \frac{1}{\int_{-t}^{t} \exp\left(-\frac{y^2}{2}\right)}. \tag{C.3}$$

The variance of this new distribution is given by

$$\begin{aligned} \sigma_Y^2 &= \int_{-t}^{t} y^2 f_Y(y)\, dy = \\ &= \frac{-2t \cdot \exp\left(-\frac{t^2}{2}\right) + \sqrt{\frac{\pi}{2}}\,\mathrm{erf}\left(\frac{t}{\sqrt{2}}\right) - \sqrt{\frac{\pi}{2}}\,\mathrm{erf}\left(-\frac{t}{\sqrt{2}}\right)}{\sqrt{\frac{\pi}{2}}\,\mathrm{erf}\left(\frac{t}{\sqrt{2}}\right) - \sqrt{\frac{\pi}{2}}\,\mathrm{erf}\left(-\frac{t}{\sqrt{2}}\right)}. \end{aligned} \tag{C.4}$$

Suppose we want to keep the variance equal to that of the non-truncated distribution. To do that, we redefine our random variable, Y, as $Z = c \cdot Y$. The probability density function of Z is now

$$f_Z(z) = \begin{cases} a_Z \exp\left(-\frac{z^2}{2c^2}\right) & \text{if } |z| < t \cdot c \\ 0 & \text{if } |z| > t \cdot c \end{cases}, \tag{C.5}$$

with $a_Z = a_Y/c$.

By definition we have that

$$\sigma_Z^2 = c^2 \sigma_Y^2 \Leftrightarrow c = \frac{\sigma_Z}{\sigma_Y}, \tag{C.6}$$

C. TRUNCATED NORMAL DISTRIBUTION

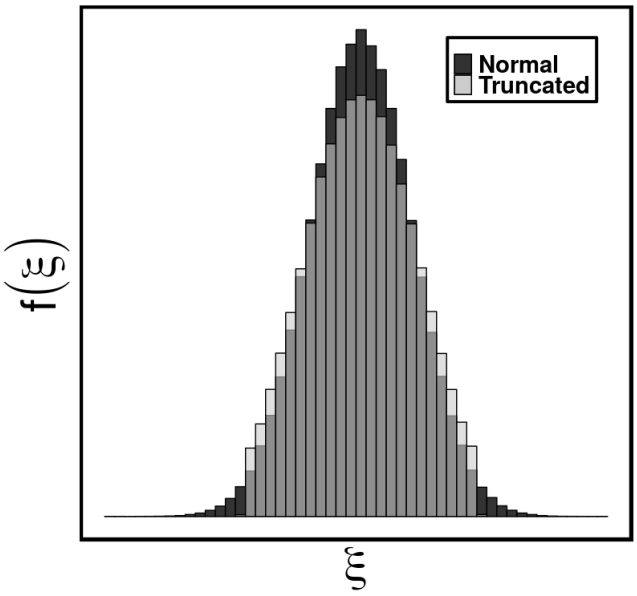

Figure C.1: Comparison between a normal distribution and its truncated version. We chose $\sigma_X = 4$, with $t = 2\sigma_X$. Note that the truncated version appears flatter. As we narrow the output interval, in other words as $|z|$ becomes smaller, the distribution becomes ever more flat, approaching a uniform one.

leaving us only with the choice of a suitable value for t.

Appendix D

Pair Potential

D.1 Cut-Off Distance

In the course of our simulation, one of the most time consuming tasks will be the calculation of the forces between inter-chain interacting pairs. Since a short ranged potential is used, after a certain distance the contribution of the force acting on the particle is negligible and doing that calculation amounts to nothing more than wasted time.

To avoid unnecessary calculations, we simply set a cut-off distance, r_c, above which the interaction is neglected. This creates a jump discontinuity at r_c, so the potential must be shifted upwards ensuring that $u(r_c) = 0$,

$$u(r_{ij}) = \begin{cases} u(r_{ij}) - u(r_c) & \text{if } r_{ij} < r_c \\ 0 & \text{if } r_{ij} \leq r_c \end{cases} . \tag{D.1}$$

This is not yet sufficient for there is a discontinuity in the force calculation when $r = r_c$. We solve this by subtracting the derivative of the function on the point which guarantees that we arrive at a smooth function

$$u(r_{ij}) = \begin{cases} u(r_{ij}) - u(r_c) - \frac{\partial u}{\partial t}\Big|_{r=r_c} (r - r_c) & \text{if } r_{ij} < r_c \\ 0 & \text{if } r_{ij} \leq r_c \end{cases} . \tag{D.2}$$

D.2 Reduced Units

When doing computer simulations, we are obliged to work in dimensionless or reduced units. By working with appropriate reduced units, where most numerical values will be the order of unity, we are able to avoid truncation and rounding errors that would be common if we were dealing with SI units at these scales. Setting up the model like this will also make it possible to re-scale it in order to describe a wider range of problems since any property can be scaled back to the appropriate physical units.

Since the particles in our system interact via a simple pair potential they can be completely specified through very few parameters such as m, σ and ε. From this definition, the units of every other physical properties can be re-scaled (table D.1) [28].

To better understand this, consider the reduced time, t, which is simply the time, t^*, in reduced units. We start with the product of our three constants, each one raised to an arbitrary power,

$$C = \sigma^a \varepsilon^b m^c . \tag{D.3}$$

Noting the units of this combination are

$$m^a J^b kg^c = m^a \left(kg \frac{m^2}{s^2} \right)^b kg^c = m^{a+2b} kg^{b+c} s^{-2b}, \tag{D.4}$$

and that our time, t^*, in SI units is given in seconds, s, we have

$$m^{a+2b} kg^{b+c} s^{-2b} = s^1 \tag{D.5}$$

where it follows that $a = 1$, $b = -1/2$ and $c = 1/2$. Remembering eq. (D.3), we can know write the reduced time as

$$t = \frac{t}{C} = t^* \left(\frac{\sigma^2 m}{\varepsilon} \right)^{-\frac{1}{2}}. \tag{D.6}$$

Table D.1: A few examples of re-scaled properties. We chose to define our SI unit properties with the '*' in order to avoid confusion when they appear in the main body of this work.

Property	**Reduced Units**
Distance (r)	$\frac{r^*}{\sigma}$
Energy (U)	$\frac{U^*}{\varepsilon}$
Force (f)	$\frac{f^* \sigma}{\varepsilon}$
Mass (m)	1
Temperature (T)	$\frac{k_B T^*}{\varepsilon}$
Time (t)	$t^* \left(\frac{\sigma^2 m}{\varepsilon} \right)^{-\frac{1}{2}}$

D.3 Periodic Boundary Conditions and Minimum Image Convention

The behaviour of a finite system such is the one we are simulating is very different from one that is, for all intents and purposes, infinite (thermodynamic limit). So, in order to accurately describe our system, and minimise surface effects, we implement periodic boundary conditions.

To do that, we surround our simulation box with images of itself. In the course of our simulations, the motion of a particle in the central box is replicated in the neighbouring boxes. This ensures that if something leaves the central box, it's image will re-enter through the opposite side, and focus will shift to it, resulting in the conservation of density in the central box (and hence in the entire system).

A consequence of defining such a system, is in the way we measure the distance between two pairs of particles. We can no longer see the central box as the only domain, but consider instead, the closest distance while accounting for all the created images (minimum image convention).

Even though this is a simple premise, and a code can be easily thought to ensure this rules are followed, attention is still required, to avoid finite-size effects from poorly chosen system size, and to perform such calculations in the most efficient way possible, since that will be required a great many deal of times. However, this will depend on many factors such as the language in which the code is written or even on the hardware it's running. We settled for a simple conditional clause

```
/*
            **** Minimum Image Convention ****
r: distance between particles
L: Box Length
half_L: L/2.0

*/

inline void nic(double& r, const double& L, const double& half_L){
    if(r > half_L){
        r -= L;
    }
    else if(x < half_L){
        r += L;
    }
}

/*
            **** Periodic Boundary Condition ****
r: distance between particles
L: Box Length

*/

inline void pbc(double& r, const double& BoxLength){
    if(r < 0){
        r -= L;
    }
    else if(x > L){
        r += L;
    }
}
```

Appendix E

Some Integrals and ODEs

E.1 First-Order Linear Ordinary Differential Equations

This type of equations take the form of

$$y'(t) + a(t)y(t) = b(t)\,, \tag{E.1}$$

with $a(t)$ and $b(t)$ being continuous functions in the interval I. In order to solve eq. (E.1), we make use of an integrating factor. We look for the antiderivative of $a(t)$, $A(t)$, and by multiplying both sides of eq. (E.1) by $\exp(A(t))$ we get

$$(y(t)\exp(A(t)))' = b(t)\exp(A(t))\,. \tag{E.2}$$

Integrating both sides reveals

$$y(t) = \exp(-A(t))\left(\int b(t)\exp(A(t))\,dt\right), \quad t \in I\,, \tag{E.3}$$

where in $\int b(t)\exp(A(t))\,dt$ we have an arbitrary constant $C \in \mathbb{R}$, determined if an initial condition, $y(t_0) = y$ with $t_0 \in I$, is provided.

E.2 Gaussian Integral

The formula for the Gaussian integral is

$$\int_{-\infty}^{+\infty} \exp(-ax^2 + bx) = \left(\frac{\pi}{a}\right)^{\frac{1}{2}} \exp\left(\frac{b^2}{4a}\right) \tag{E.4}$$

where a is a positive constant and b is an arbitrary complex variable.